The Journal of Chemical Physics

Vibronic dynamics resolved by global and target analysis of ultrafast transient absorption spectra

Cite as: J. Chem. Phys. **155**, 114113 (2021); https://doi.org/10.1063/5.0060672
Submitted: 21 June 2021 . Accepted: 03 September 2021 . Published Online: 21 September 2021

Ivo H. M. van Stokkum, Miroslav Kloz, Dario Polli, Daniele Viola, Jörn Weißenborn, Ebo Peerbooms, Giulio Cerullo, John T. M. Kennis, et al.

AIP Publishing

The Journal of Chemical Physics ARTICLE scitation.org/journal/jcp

Vibronic dynamics resolved by global and target analysis of ultrafast transient absorption spectra

Cite as: J. Chem. Phys. 155, 114113 (2021); doi: 10.1063/5.0060672
Submitted: 21 June 2021 • Accepted: 3 September 2021 •
Published Online: 21 September 2021

Ivo H. M. van Stokkum,[1,a)] Miroslav Kloz,[2] Dario Polli,[3] Daniele Viola,[3] Jörn Weißenborn,[1] Ebo Peerbooms,[1] Giulio Cerullo,[3] and John T. M. Kennis[1]

AFFILIATIONS

[1] Department of Physics and Astronomy and LaserLaB, Faculty of Science, Vrije Universiteit Amsterdam, De Boelelaan 1081, 1081 HV Amsterdam, The Netherlands
[2] Institute of Physics, ELI Beamlines, Academy of Sciences of the Czech Republic, CZ-18221 Prague, Czech Republic
[3] IFN-CNR, Department of Physics, Politecnico di Milano, Piazza Leonardo da Vinci 32, 20133 Milano, Italy

[a)] **Author to whom correspondence should be addressed:** i.h.m.van.stokkum@vu.nl. **Telephone:** +31205987868

ABSTRACT

We present a methodology that provides a complete parametric description of the time evolution of the electronically and vibrationally excited states as detected by ultrafast transient absorption (TA). Differently from previous approaches, which started fitting the data after ≈100 fs, no data are left out in our methodology, and the "coherent artifact" and the instrument response function are fully taken into account. In case studies, the method is applied to solvents, the dye Nile blue, and all-trans β-carotene in cyclohexane solution. The estimated Damped Oscillation Associated Spectra (DOAS) and phases express the most important vibrational frequencies present in the molecular system. By global fit alone of the experimental data, it is difficult to interpret in detail the underlying dynamics. Since it is unfeasible to directly fit the data by a theoretical simulation, our enhanced DOAS methodology thus provides a useful "middle ground" where the theoretical description and the fit of the experimental data can meet. β-carotene in cyclohexane was complementarily studied with femtosecond stimulated Raman spectroscopy (FSRS). The fs–ps dynamics of β-carotene in cyclohexane in TA and FSRS experiments can be described by a sequential scheme S2 → hot S1 → S1′ → S1 → S0 with lifetimes of 167 fs (fixed), 0.35, 1.1, and 9.6 ps. The correspondence of DOAS decaying concomitantly with hot S1 and the Species Associated Difference Spectra of hot S1 in TA and FSRS suggest that we observe here features of the vibrational relaxation and nuclear reorganization responsible for the hot S1 to S1 transition.

INTRODUCTION

Transient absorption (TA) spectroscopy is widely used to follow photophysical dynamics in systems ranging from relatively simple molecules[1–8] to complex supramolecular systems involved in photosynthesis.[9–15] When a molecule is impulsively excited by a broadband pulse, vibrational wavepackets of Franck–Condon active modes can be launched (according to a semi-classical model) in the ground and excited state potential energy surfaces (PESs).[16–20] Photoexcitation thus gives rise to superimposed population and vibrational coherence dynamics in TA spectra. Whether vibrational wavepackets are generated on the ground or excited state PES depends on the properties (spectrum, duration, and chirp) of the exciting pulse.[21–26] Vibrations can be assigned to the ground or excited state based on the probe wavelength dependence of their amplitude and phase, where a node in the amplitude, accompanied by a corresponding phase flip, can mark the minimum of the electronic PES on which the wavepacket is oscillating.[5–7,27–32]

Virtually, all ultrafast TA experiments present very intense signals around zero delay, which are due to non-resonant interactions between pump and probe pulses and are commonly referred to as the "coherent artifact" (CA). These signals may have different origins, such as scattering of the pump pulse along the probe propagation direction due to a transient population grating, cross-phase modulation between pump and probe pulses, and two-photon absorption.[33–37] Many analyses neglect the CA and only start to fit the data at a delay for which it is concluded. In this way, they miss important information on the early time dynamics and on the phases of the

observed oscillations because time zero is uncertain. This severely limits the interpretation of the experimental data. In those analyses of TA spectra, population and oscillation dynamics are most often treated separately. First, the population dynamics are fitted and subtracted from the data, and then the residual oscillatory signals well after the CA duration are analyzed. Time traces at single detection wavelengths are either Fourier transformed or fitted with damped cosines.[1–3,8,27,29,38,39] Next, for a few dominant frequencies, the amplitude and phase profiles are plotted as a function of the detection wavelength.

Previously, we introduced a generalized global and target analysis methodology enabling one to resolve simultaneously the contributions of the different electronically and vibrationally excited states from the complete TA dataset.[40] The method was successfully applied to cryptophyte light harvesting proteins[40,41] and perylenediimides.[42] Similar methods to estimate wavepacket dynamics parameters have independently been developed.[8,43,44] Here, we present an important improvement of our method that fully incorporates the description of the CA in the global analysis, allowing us to exploit all the available data and to enhance the time resolution. In particular, the analytical parametric description of the CA enables us to estimate the time zero parameter, which represents the time of the maximum of the Instrument Response Function (IRF). We apply our novel method first to the solvent cyclohexane and to the dye Nile blue where vibrational wavepackets have been demonstrated already in 1990.[45,46] Simple off-resonant and resonant Damped Oscillation Associated Spectra (DOAS) are simulated, which mimic the experimentally estimated DOAS in cyclohexane and Nile blue and thus aid in their interpretation. Then, in a case study, we comprehensively analyze high quality broadband TA data from all-trans β-carotene in cyclohexane solution.[1,2,38,47] We demonstrate that we can resolve and describe the vibronic dynamics in the time domain.

Complementary to broadband TA spectroscopy is femtosecond stimulated Raman spectroscopy (FSRS).[48–53] Although the time resolution of FSRS is lower [typically the IRF is ≈125 fs full width at half maximum (FWHM)], the spectral selectivity is superior, allowing detailed observation of the intermediates involved in the fs–ps dynamics of β-carotene in cyclohexane. Thus, by combining the DOAS analysis of TA and FSRS experiments, we aim to provide a consistent interpretation of the vibronic dynamics of β-carotene in cyclohexane.

MATERIALS AND METHODS

Modeling and parameter estimation

Our model is an extension of the generalized global and target analysis methodology presented before,[40] which now fully takes into account the CA and the IRF. For the sake of completeness and in order to enable the reader to understand and apply the model without the need to refer to other papers, we present here the full model. In target analysis[54,55] of TA data, the inverse problem is to determine the number of electronically excited states (N_{states}) present in the system, to estimate their populations $c_l^S(t)$ (superscript S stands for species), and the species' spectral properties, the Species Associated Difference Spectra [$SADS_l(\lambda)$], where λ is the wavelength. The evolution of the ground and excited state vibrational wavepackets created by the short laser pulse is described with a superposition of damped oscillations. The amplitude of a damped oscillation $\cos(\omega_n t)\exp(-\gamma_n t)$ as a function of the detection wavelength constitutes a Damped Oscillation Associated Spectrum [$DOAS_n(\lambda)$] with an accompanying wavelength dependent phase $\varphi_n(\lambda)$. When the vibrational evolution can be considered independently from the electronic evolution (Born–Oppenheimer approximation), we arrive at a superposition of the electronic and vibrational contributions to the Time Resolved Spectra (TRS),

$$TRS(t,\lambda) = \sum_{l=1}^{Nstates} c_l^S(t',\theta) SADS_l(\lambda) + \sum_{n=1}^{Nosc} DOAS_n(\lambda)\cos(\omega_n t' - \varphi_n(\lambda))\exp(-\gamma_n t'),$$

where the populations are determined by an unknown compartmental model, which depends upon the unknown kinetic parameters θ. In the target analysis, constraints on the $SADS$ are needed to estimate all parameters θ and $SADS_l(\lambda)$. t' indicates that the actual model function still has to take into account the IRF. Previously,[40] we neglected the consequences of the IRF for the damped oscillations. In the novel methodology presented below, we derive an analytical expression for the convolution of the IRF with a damped oscillation. In addition, we describe the CA with the zeroth, first, and second derivatives of the IRF.[33] The advantage of phenomenologically using the IRF derivatives is that no further theory is needed.

Typically, a Gaussian shaped IRF is adequate, with parameters μ for the time of the IRF maximum and Δ for the full width at half maximum (FWHM) of the IRF,

$$IRF(t) = \frac{1}{\tilde{\Delta}\sqrt{2\pi}}\exp(-\log(2)(2(t-\mu)/\Delta)^2) = \frac{1}{\tilde{\Delta}\sqrt{2\pi}}\exp\left(-\left(\frac{t-\mu}{\sqrt{2}\tilde{\Delta}}\right)^2\right),$$

where $\tilde{\Delta} = \Delta/(2\sqrt{2\log(2)})$. The convolution (indicated by an *) of this IRF with an exponential decay (with decay rate k) yields an analytical expression, which facilitates the estimation of the decay rate k and the IRF parameters μ and Δ,

$$c^D(t,k,\mu,\Delta) = \exp(-kt) * IRF(t) = \frac{1}{2}\exp(-kt)\exp\left(k\left(\mu + \frac{k\tilde{\Delta}^2}{2}\right)\right) \times \left\{1 + \mathrm{erf}\left(\frac{t-(\mu+k\tilde{\Delta}^2)}{\sqrt{2}\tilde{\Delta}}\right)\right\}.$$

This expression can be written more elegantly as

$$c^D(t,k,\mu,\Delta) = \exp\left(-\left(\frac{t-\mu}{\sqrt{2}\tilde{\Delta}}\right)^2\right)\mathrm{erfc}\,x(z),$$

where the scaled complementary error function $\mathrm{erfc}\,x(z)$ is defined as $\mathrm{erfc}\,x(z) = \exp(z^2)\mathrm{erfc}(z)$ with $z = -\frac{t-(\mu+k\tilde{\Delta}^2)}{\sqrt{2}\tilde{\Delta}}$. Note that c^D is the product of the shape of the Gaussian IRF and $\mathrm{erfc}\,x(z)$. Thus, it can be considered a **doubly scaled** complementary error function. Now

to derive the convolution of the IRF with a damped oscillation, we substitute $\gamma + i\omega$ for k to find

$$c^D(t,\gamma,\omega,\mu,\Delta) = \exp\left(-\left(\frac{t-\mu}{\sqrt{2}\tilde{\Delta}}\right)^2\right) w(-z),$$

where the Faddeeva function $w(-z)$ is defined as $w(-z) = \exp(-z^2)\mathrm{erfc}(iz)$ with $z = -\frac{t-(\mu+(\gamma+i\omega)\tilde{\Delta}^2)}{\sqrt{2}\tilde{\Delta}}$. Note that c^D is now the product of the shape of the Gaussian IRF and $w(-z)$. This ***scaled*** Faddeeva function is computed with a modification of the TOMS680 algorithm of Poppe and Wijers.[56] Alternatively, it could be implemented using the Faddeeva package.[57] Representative examples of the cosine and sine oscillations with a period of 22 fs (frequency of 1524 cm^{-1}) and FWHM of the IRF Δ of 14 fs are depicted in Fig. 1. Note that after the first cycle, the convolution with the IRF results in a smaller amplitude oscillation because the IRF width is comparable to the period of the oscillation. Higher frequencies will have even smaller amplitudes, whereas lower frequencies are less affected. The damping rate of $\gamma = 2.8\ \mathrm{ps}^{-1}$ results in a slowly decreasing amplitude of the oscillations on the ps time scale.

When the compartmental model consists of independently decaying species, with populations $c_l^D(t,k_l,\mu,\Delta)$ (superscript D stands for decay), their spectra are termed $DADS_l(\lambda)$ (Decay Associated Difference Spectra). The interrelation between the DADS and SADS is expressed in the following matrix equation:[40]

$$C^D(\theta,\mu,\Delta)\cdot DADS^T = C^S(\theta,\mu,\Delta)SADS^T.$$

Here, the matrix $C^D(\theta,\ \mu,\Delta)$ contains in its lth column the decay $c_l^D(t,k_l,\mu,\Delta)$ and the matrix $C^S(\theta,\ \mu,\Delta)$ contains in its columns the populations $c_l^S(t)$ of the compartmental model used.

The superposition model for the $TRS(t,\lambda)$ is given by the matrix formula

$$TRS = C^S(\theta,\mu,\Delta)\cdot SADS^T + \cos(\omega,\gamma,\mu,\Delta)\cdot A^T + \sin(\omega,\gamma,\mu,\Delta)\cdot B^T + IRF(\mu,\Delta')\cdot IRFAS^T.$$

Here, the matrices $\cos(\omega,\gamma,\ \mu,\Delta)$ and $\sin(\omega,\gamma,\ \mu,\Delta)$ contain the damped oscillations, and the matrices A and B comprise their amplitudes. In order to limit the number of free parameters, we assume the wavelength independence of the eigenfrequency ω_n and of the damping rate γ_n. Because the cosine and the sine damped oscillations are the real and imaginary parts of $\exp(-(\gamma_n + i\omega_n)t)$, the model functions for the nth damped oscillation are computed as the real and imaginary parts of $c^D(t,\gamma_n,\omega_n,\ \mu,\Delta)$.

The final term, which describes the coherent artifact, contains a matrix $IRF(\mu,\Delta')$ with the zeroth, first, and second derivatives of the IRF.[33] Experimentally, we found that the width $\Delta' > \Delta$, as will be discussed below. Associated with each IRF derivative are the columns of the $IRFAS$ matrix. The CA is described by the $IRF(\mu,\Delta')\cdot IRFAS^T$ term plus a number of strongly damped oscillations, some of which are time-reversed to account for pre-zero oscillations due, for example, to pump-perturbed free induction decay.[36,58]

The dimensions of the matrices are collated in Table I.

The intrinsically nonlinear parameters of this model are the vector θ (containing the microscopic decay rates and inputs to the compartments x_l, detailed in Ref. 40), the IRF parameters (μ,Δ,Δ'), and the N_{osc}-vectors ω,γ. The number of vibrational modes that can reliably be resolved N_{osc} critically depends on the signal-to-noise ratio of the measured $TRS(t,\lambda)$. The conditionally linear parameters are the matrices $SADS$, A, B, and $IRFAS$. Typically, there are nλ times more conditionally linear parameters than intrinsically nonlinear parameters, see Table I.

Because the phase $\varphi_n(\lambda)$ is not a conditionally linear parameter, the DOAS and phases cannot be fitted directly but must be computed from the estimated cosine and sine amplitude matrices A and B. The nth $DOAS_n$ at wavelength λ_j is computed as

$$DOAS_{jn} = \sqrt{A_{jn}^2 + B_{jn}^2}.$$

The reconstruction of the phase φ_n, called phase unwrapping, the parameter estimation, and the residual analysis have been described in Ref. 40.

When fitting data that contain a dominant CA, a weight of 0.2 is applied to the CA part of the data, to avoid the occurrence of spurious oscillations at later times.

To aid the interpretation of the large amount of estimated parameters, it is instructive to synthesize the total CA contribution to the signal by adding the $IRF(\mu,\Delta')\cdot IRFAS^T$ term and the

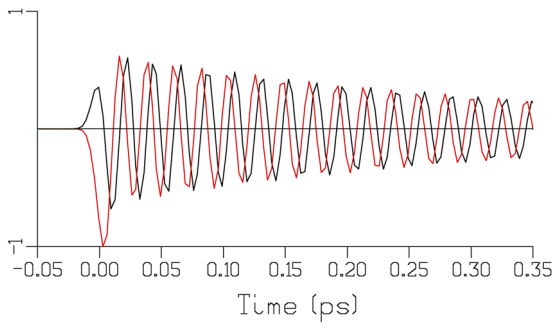

FIG. 1. Cosine (black) and sine oscillations (red) with a period of 22 fs (frequency of 1524 cm^{-1}) and damping rate $\gamma = 2.8\ \mathrm{ps}^{-1}$. The FWHM of the IRF Δ is 14 fs.

TABLE I. Dimensions of the matrices, nt and nλ are the number of times and wavelengths of the TRS matrix.

	Nrow	Ncol
TRS	nt	nλ
$C^S(\theta,\ \mu,\Delta)$	nt	N_{states}
SADS	nλ	N_{states}
$\mathrm{Cos}(\omega,\gamma,\ \mu,\Delta)$	nt	N_{osc}
A	nλ	N_{osc}
$\mathrm{Sin}(\omega,\gamma,\ \mu,\Delta)$	nt	N_{osc}
B	nλ	N_{osc}
$IRF(\mu,\Delta')$	nt	3
$IRFAS$	nλ	3

strongly damped oscillations that are ascribed to the CA. Likewise, a solvent impulsive stimulated Raman scattering (ISRS) signal can be synthesized by adding all the solvent ISRS oscillations. These syntheses allow us to judge the applicability of the methodology.

Transient absorption measurements

We use our improved DOAS model to analyze and compare broadband TA measurements from two different laboratories. Measurements of all-trans β-carotene in cyclohexane solution have been described in Polli *et al.*[1] Briefly, broadband sub-10-fs excitation pulses, generated by a non-collinear optical parametric amplifier (NOPA) pumped by an amplified Ti:sapphire laser at 1 kHz, were tuned to a 560 nm central wavelength. The high energy tail of a typical pulse spectrum [solid black line in Fig. S1(A)] overlaps with the low energy absorption of all-trans β-carotene [red line in Fig. S1(A)]. The probe pulse, which is an attenuated and delayed replica of the pump, following transmission by the sample is dispersed on the spectrometer, and TA spectra, obtained chopping the pump at 500 Hz frequency, are measured as a function of wavelength and delay, $TRS(t,\lambda)$.

TA spectra were measured in steps of 3 fs until 1.2 ps and then in larger time steps until 30 ps. The wavelength resolution was 0.85 nm, and the covered wavelength interval ranged from 491 to 678 nm. More recently, the experiment has been repeated with 3 fs time resolution over a 12 ps time scale (instead of 1.2 ps) in order to monitor the complete decay of the oscillations.

In Ref. 2, three different broadband TA measurements of all-trans β-carotene in cyclohexane solution are described: (1) of the solvent only (called the CA measurement); (2) "off-resonant" excitation of β-carotene in cyclohexane with an ultrashort pulse generating a ground state (GS) vibrational coherence via impulsive stimulated Raman scattering (ISRS); a repeat measurement of (2); and (3) a three-pulse experiment, whereby a resonant pump pulse at 460 nm precedes by 2 ps the ISRS pump. The spectrum of the ISRS pulse slightly overlaps with the β-carotene absorption [cf., Figs. S2(B) and S2(C)], thus selectively exciting the redmost absorbing β-carotenes.

Measurements of Nile blue in methanol have been described by Liebel *et al.*[38] Table II collates the characteristics of all the TA experiments analyzed.

FSRS measurements

Femtosecond stimulated Raman experiments were performed with the watermarking nearly baseline-free stimulated Raman method reported previously.[51,59–61] Spectral watermarking, detailed by Kloz *et al.*,[51] recombines several FSRS experiments with slightly shifted Raman pulses, thus allowing robust rejection of baselines and fixed-pattern-noise. Briefly, the Raman pump (800 nm, ≈5 μJ, 100 μm spot diameter) and the Raman probe (≈840–960 nm, 30 μm spot diameter) were spatiotemporally overlapped at the sample position. β-carotene in cyclohexane, circulated in a 1 mm thick quartz flow cell, was excited with a low intensity (80 nJ, 200 μm spot diameter) 495 nm actinic pulse focused on the sample. The Raman pump was prepared by spectral filtering of the 790 nm centered 90 nm FWHM wide laser pulse.[59] The Raman probe was generated by splitting part of beam from the laser, converting it to 1450 nm by an optical parametric amplifier and then driving supercontinuum generation in a moving calcium fluoride plate. The resulting white light was filtered by 1 cm of water to remove the 1450 nm component. The probe light was dispersed by a spectrograph (Acton SP2150, Princeton Instruments) and detected by a 1024-pixel back-thinned FFT-CCD detector (S7030-1007, Hamamatsu). The FWHM of the IRF was ≈127 fs. Here, we analyze time gated spectra from 820 to 2100 cm^{-1} and from −1 to 100 ps.

RESULTS AND DISCUSSION

The coherent artifact in solvent

Broadband TA measurements of pure cyclohexane solvent have been described in Ref. 2. The time step used was 3.33 fs.

The CA in cyclohexane straddles time zero [Fig. 2(a)], with amplitudes up to 30 mOD, and it extends until ≈±0.1 ps relative to the location of the maximum of the IRF. The overall rms error of the fit was 0.36 mOD. The estimated FWHM of the CA was 42 fs [Fig. 2(c), black], while the FWHM of the IRF was fixed at 14 fs. These characteristics have been collated in Table II as well and, henceforth, will no longer be quoted. The CA is dominated by the second derivative of the IRF temporal profile [blue in Figs. 2(c) and 2(d)]. Following the artifact, we observe oscillations with a total amplitude of about 1 mOD, with representative zoom ins depicted

TABLE II. Overview of the TA experiments, their conditions, and some characteristics: pump and probe wavelength region, FWHM of the IRF Δ and CA Δ', the rms error, a rough estimate of the total oscillatory amplitude, and the SADS extremum.

Sample	λ_{pump} (nm)	λ_{probe} (nm)	Δ (fs)	Δ' (fs)	$\lambda_{(p)repump}$ (nm)	Time step (fs)	rmse (mOD)	osc amp (mOD)	SADS (mOD)	Figures
Cyclohexane[2]	530–650	500–850	14	34		3.33	0.51	1		Figure 2 and Fig. S3
Nile blue in methanol[38]	800 (c)	510–860	14	42		2.8	0.36	3	−0.75	Figure 3 and Fig. S6
β-carotene in cyclohexane[1]	490–750	490–750	14	43		3.0	0.81	3	77	Figure 6 and Fig. S10
β-carotene in cyclohexane, this work	530–750	530–750	14	32		3.0	0.29	2.5	5.6	Figures S16 and S17
β-carotene in cyclohexane[2]	530–650	500–850	14	36		3.33	0.054 0.041	1 0.65	6.2 3.7	Figure 7, Figs. S12 and S14
β-carotene in cyclohexane[2]	530–650	500–850	14	36	460 nm at −2 ps	3.33	0.114	1.5	74	Figure S19

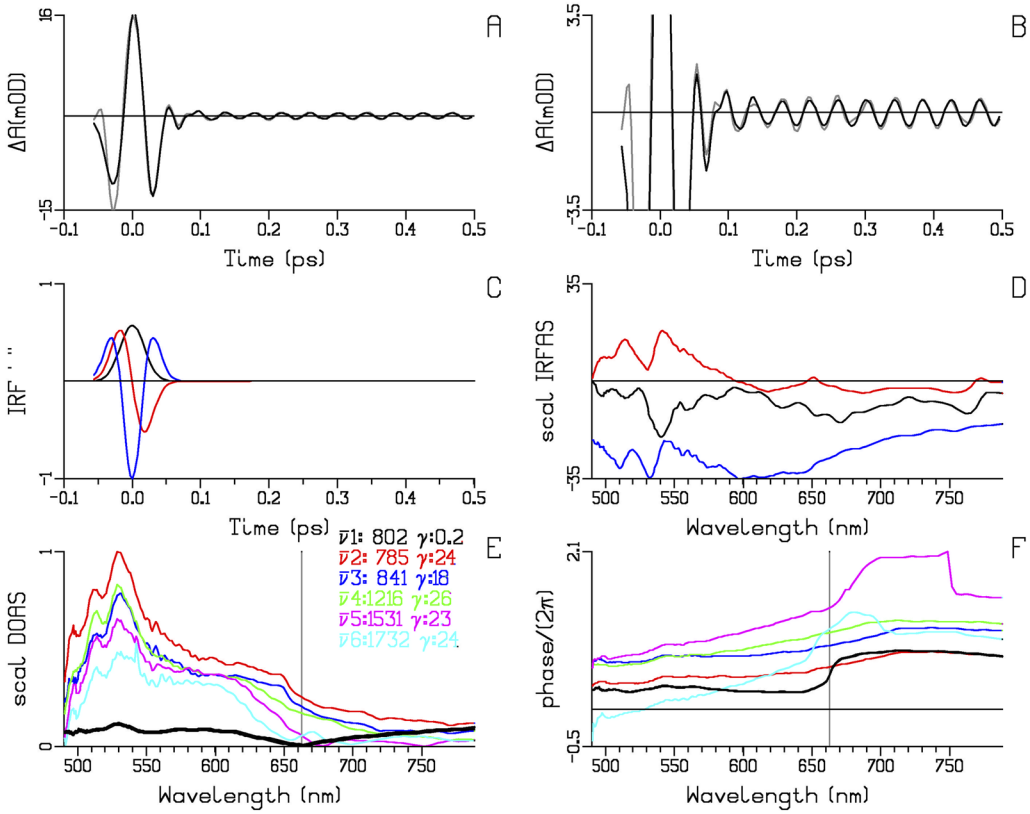

FIG. 2. DOAS analysis of cyclohexane excited with a 12 fs pulse centered at ≈570 nm and probed with a 5 fs pulse at 660 nm. (a) and (b) Analysis at 759 nm, zoom from −0.1 to 0.5 ps (after the maximum of the IRF) of the data (in mOD, gray) and the fit (black). Note the different vertical scales: the CA is clearly visible in (a) but clipped in (b). (c) CA IRF zeroth, first, and second derivative (black, red, and blue) (d) IRFAS. Scaling of the IRFAS is such that the product of the IRFAS and the IRF derivative is the contribution to the fit. (e) and (f) Overview of selected DOAS and phases. Frequencies $\bar{\nu}n$ (in cm^{-1}) (where n is the DOAS number) and damping rates γ (in ps^{-1}) are written in the legend of panel (e) using the appropriate color. (e) Estimated DOAS, scaled for comparison. (f) Estimated phase profiles of the DOAS. The gray vertical lines at 663 nm in panels (e) and (f) are discussed in the text.

in Fig. 2(b) and Fig. S3(C). At 759 nm, the IRFAS [Fig. 2(d)] are relatively small. The power spectrum of the signal after 0.1 ps (relative to the IRF) shows a dominant peak near 800 cm^{-1} [Fig. S3(C), inset], assigned to the well-known cyclohexane Raman band at 802 cm^{-1} excited by ISRS. In a global analysis of all data, five damped oscillations with damping rates of about 25 ps^{-1} were resolved (No. 2–No. 6), but only the first 802 cm^{-1} damped oscillation (damping rate of 0.2 ps^{-1}) extends well beyond 0.2 ps, and its DOAS and phase are depicted in black in Figs. 2(e) and 2(f) and Figs. S3(G)–S3(I). A clear node accompanied by an $\approx\pi$ phase jump is present at 663 nm, near the peak of the probe pulse spectrum [Fig. S2(C), green]. This is in agreement with the off-resonance ISRS mechanism in which the generated ground state vibrational coherence modulates the refractive index of the medium, resulting in a periodic red- and blue-shift of the probe pulse spectrum.[62–64] The maximum at ≈530 nm could be interpreted as anti-Stokes Raman scattering off the pump, which showed a secondary maximum at ≈560 nm [Fig. S2(C), purple]. Note that the residual of the fit [Fig. S3(F)] still shows some oscillatory structure, but the power spectrum has a maximum less than 2% of that in Fig. S3(C) and it no longer shows a dominant peak. Thus, this huge body of data can be well described with the help of our parametric model. Below, we will demonstrate that we can simulate the properties of the 802 cm^{-1} DOAS and phase profile.

Nile blue in methanol

We next turn to the study of the coherent oscillatory dynamics in a simple dye molecule, Nile blue in methanol excited by a 10-fs pulse centered at 800 nm. The pulse is nearly off resonance with the absorption ($\lambda_{max,abs}$ 626 nm) of the molecule; however, its spectrum is so broad that it still manages to excite it with a tail. The single retrieved SADS [Fig. 3(a)] is a sum of the ground state (GS) bleaching and stimulated emission (SE) from the excited state. The observed lifetime is much longer than the 2 ps time scale; according to the literature, it is 1.4 ns.[65] The CA straddles time zero [Fig. 3(b)], with amplitudes up to 90 mOD, while the total amplitude of the oscillations starts at about 3 mOD, representative zoom ins are depicted in Figs. S4(C) and S4(F). The power spectrum peaks at 592 cm^{-1}. The DOAS in Figs. 3(c) and 3(d) [see also Figs.

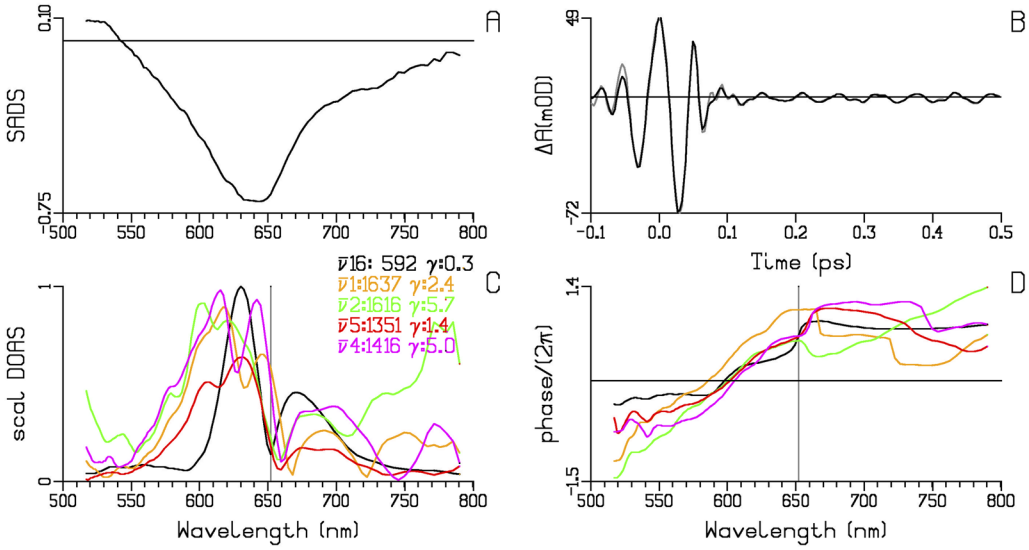

FIG. 3. DOAS analysis of Nile blue in methanol excited with a 10 fs pulse centered at 800 nm. (a) Estimated SADS. (b) Zoom from −0.1 to 0.5 ps (after the maximum of the IRF) of the 630 nm data (in mOD, gray) and the fit (black). (c) and (d) Overview of the five largest estimated DOAS and phases. Frequencies $\bar{\nu}n$ (in cm^{-1}) (where n is the DOAS number) and damping rates γ (in ps^{-1}) written in the legend of panel (c) using the appropriate color. (c) Estimated DOAS, scaled for comparison. (d) Estimated phase profiles of the DOAS. The gray vertical lines at 652 nm in panels (c) and (d) are discussed in the text.

S4(G)–S4(I)] show nicely the shape of the GS bleaching plus also the shape of the SE (maxima from 660 to 680 nm, in accordance with $\lambda_{max,emiss}$ 668 nm). The 16th DOAS, 592 cm^{-1}, decays with about 0.3 ps^{-1} [black in Figs. 3(c) and 3(d)]. A node accompanied by an $\approx\pi$ phase jump is present at 652 nm. Thus, the phase of the oscillations in the SE and in the bleaching, above and below 652 nm, differs by about π [Fig. 3(d)]. The contribution of the damped oscillations to the fit and the quality of the fit are demonstrated in Fig. S5. The next four largest DOAS decay with rates between 1.4 and 5.7 ps^{-1}. The 18 estimated DOAS frequencies [Figs. S4(G), S4(J), and S4(M)] well correspond to the largest amplitude modes estimated from a frequency domain resonance-Raman spectrum.[66] No amplitude correction is needed for high frequencies, since our model function already takes into account the convolution of the IRF and the damped oscillation. This DOAS analysis of Nile blue demonstrates that both the eigenfrequencies (modes), the wavelength dependent amplitudes and phases, and the decay rates of the damped oscillations can be reliably estimated. Below, we will demonstrate that we can simulate the properties of the 592 cm^{-1} DOAS and phase profile.

The DOAS results can be compared to a conventional Fourier transform analysis of the residuals, depicted in Fig. S6. The power spectra (insets) show a wavelength dependent pattern of many peaks. To take into account the convolution with the IRF, an amplitude correction would be needed for frequencies above ≈1000 cm^{-1}, as demonstrated in Ref. 38. The main peaks are near 588 and 879 cm^{-1} with a handful of smaller peaks around 1500 cm^{-1}. To further quantify the power spectra at all wavelengths, one would need to fit them with a global parametric model with spectral bands. The DOAS analysis directly fits all the measured data in the time domain, not discarding the data before 100 fs, and the shape of the peaks is described by the damped (co)sine, from which the wavelength dependent amplitude and phase are estimated. The main peaks in the power spectra near 588 and 879 cm^{-1} are now described by DOAS Nos. 15 and 16 [Figs. S4(M)–S4(O)] and by DOAS Nos. 10 and 11 [Figs. S4(J)–S4(L)], respectively. The smaller peaks around 1500 cm^{-1} are now described by DOAS Nos. 1–5 [Figs. S4(G)–S4(L)].

Simulations

The ≈802 cm^{-1} DOAS and phase that were estimated in Fig. 2 have been attributed to off-resonance ISRS of cyclohexane.

Using the theory of Kumar *et al.*,[67] the DOAS and phase characteristics have been simulated using the parameters of Table III. In this formalism, the contribution of vibrational overtones to the TA spectrum expresses the pump-induced polarization in the form of a two-time correlation function. This correlation function can be analytically evaluated in the case of undamped nuclear motion and takes the form of a correction to the equilibrium absorption spectrum induced by the pump pulse. For the simulation results shown, the cosine and sine contributions to the first vibrational overtone have been simulated in the low-temperature limit, further improving the tractability of the expressions.

TABLE III. Parameters used to simulate Figs. 4 and 5.

Simulation	Pulse center wavelength (nm)	Pulse duration (fs)	Transition wavelength (nm)
Figure 4	662	4.5	162
Figure 5	636	9	635

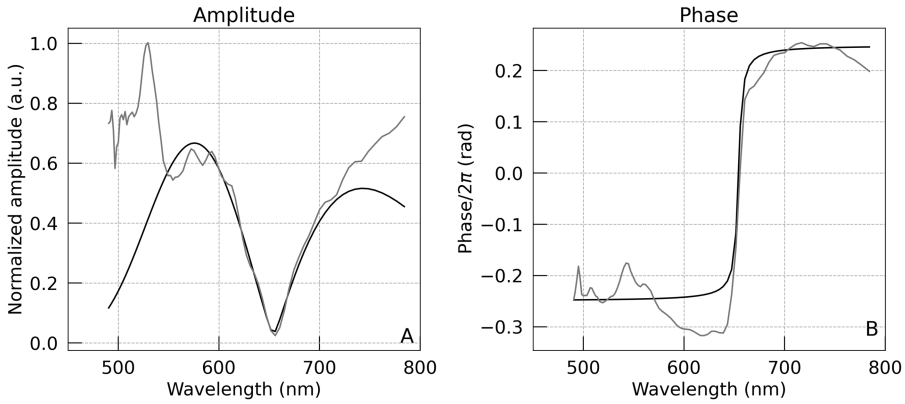

FIG. 4. Simulations (black) of estimated (gray) cyclohexane 802 cm^{-1} DOAS (a) and phase/2π (b) from Fig. 2. The DOAS has been treated as an off-resonance ISRS phenomenon. Parameter values for the simulation were estimated based on the best agreement with the slope of the phase jump and the location of the amplitude minimum and are collated in Table III.

Since the absorption of cyclohexane occurs mostly in the UV band,[68] the DOAS from the TA experiment has been modeled as an off-resonance Raman interaction with the pump pulse. The model has been fitted against the DOAS cosine and sine data from the TA experiment, resulting in the estimated parameters from Table III. The most characteristic of the "Liebel" DOAS in Fig. 4(a) is the node near 662 nm accompanied by a π phase jump. This jump can be down or up. It can be well simulated with the help of a probe spectrum that has its maximum at 662 nm.

Finally, the 592 cm^{-1} DOAS from Nile blue in methanol [No. 16 in Figs. 3(c) and 3(d)] has been simulated using the same theory (Fig. 5). In line with Ref. 67, the oscillatory signal is dominated by the excited state contribution [Figs. S7(B)–S7(D)]. We used the parameters given in Table III; other parameters in the model are the dimensionless electronic state displacement D and the ground state population fraction Ng after the interaction with the pump pulse. For the results shown in Fig. 5, these parameters were estimated at D = 0.515 and Ng = 0.99. Consequently, the excited state population fraction equals 0.01. The model used for simulating the DOAS is currently only able to simulate a single vibrational mode coupled to a single electronic transition. Qualitative agreement with the data can be achieved, but similar results are obtained for a range of the parameters. As such, the simulation results are indicative of the properties of the features observed in the DOAS but do not yet provide conclusive information. It would be interesting to simulate the DOAS and IRFAS with the help of more detailed theories employing a high-dimensional system Hamiltonian.[28,33–35,69,70]

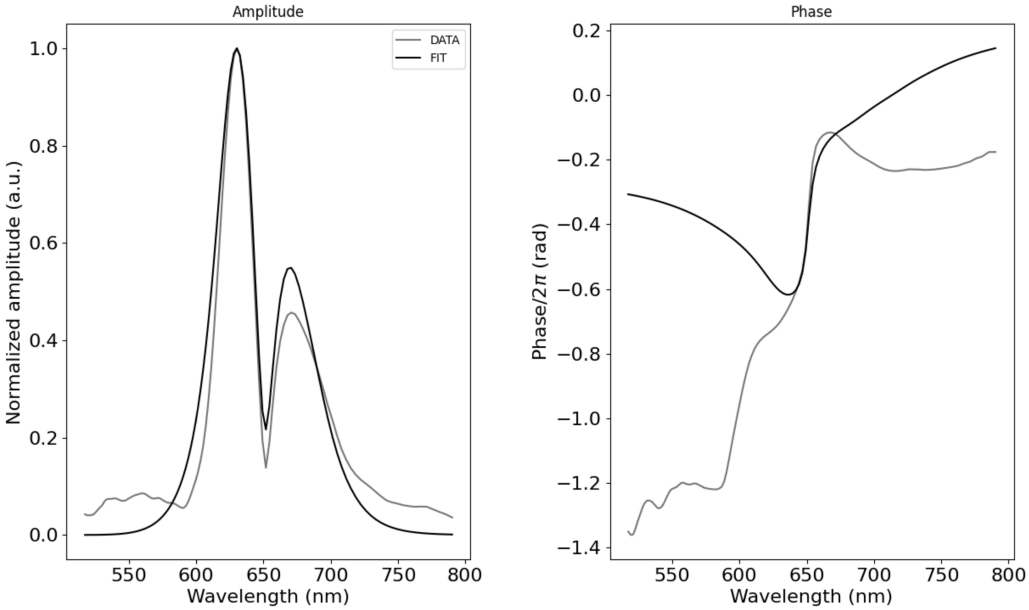

FIG. 5. Simulations (black) of estimated (gray) Nile blue 592 cm^{-1} DOAS (left) and phase (right). Simulation parameters are obtained by simultaneously fitting the cosine and sine contributions to the corresponding DOAS components. Optimized cosine and sine simulation parameters are then used to reconstruct the amplitude and phase profiles.

All-trans β-carotene in cyclohexane

We next discuss the DOAS observed in β-carotene in cyclohexane solution in a broadband TA experiment performed with 7 fs pulses centered at 562 nm [Fig. S1(A)]. The amplitude of the oscillations starts at about 3 mOD [Fig. S10(F)].

The photophysics of β-carotene can be described by a three-state model, where the first excited state S1 is optically dark, as it has the same symmetry as the ground state S0, so that S0 → S2 is the first allowed transition. A sequential kinetic scheme S2 → hot S1 → S1 → S0 was used to describe the excited state dynamics [Fig. S10(A)]. The S2 SADS [black in Fig. 6(a)] shows SE, with a peak at 570 nm, and S2 decays to hot S1 in 168 fs. The hot S1 SADS [red in Fig. 6(a)] shows a broad excited state absorption (ESA) with a maximum at 570 nm, which decays to vibrationally relaxed S1 in 0.38 ps, thereby losing part of the redmost components from 570 to 670 nm and gaining some spectral weight from 530 to 560 nm [cf., the red DADS in Fig. 6(b)]. The relaxed S1 SADS [blue in Fig. 6(a)] peaks at 560 nm and decays back to S0 in 9 ps. Thirteen damped oscillations were needed to fit the vibrational evolution up to the noise level, cf., Fig. S8. The first left and right singular vectors of the residual matrix are depicted in Fig. S9. No obvious structure is discernible. Thus, we conclude that the maximum number of reliably resolvable damped oscillations with this signal-to-noise level is 13. An overview of 11 estimated DOAS and phases is given in Figs. 6(c)–6(f). The amplitude of the 804 cm^{-1} DOAS [No. 6, black in Figs. 6(e) and 6(f)], assigned to the cyclohexane solvent, is comparable to that of Nos. 7–11. DOAS No. 4 [1003 cm^{-1}, damping rate 1.7 ps^{-1}, green in Figs. 6(c) and 6(d)] shows a node at 563 nm, accompanied by an $\approx\pi$ phase jump [cf., the gray vertical lines in Figs. 6(c) and 6(d)]. Note that the red DADS that represents the vibrational cooling in hot S1 crosses zero near 563 nm [Fig. 6(b)]. DOAS No. 8 [500 cm^{-1}, damping rate 0.9 ps^{-1}, blue in Figs. 6(e) and 6(f)] shows a node accompanied by an $\approx\pi$-phase jump at 523 nm [cf., the gray vertical lines in Figs. 6(c) and 6(d)]. Below we will discuss possible interpretations of these observations.

Liebel and Kukura[2] also measured β-carotene in cyclohexane, but here, due to the nearly off-resonant condition, the CA was relatively more intense (Fig. S11), and the SADS of the relaxed S1 state had a maximum of only 6.2 mOD [Fig. 7(a)], whereas in

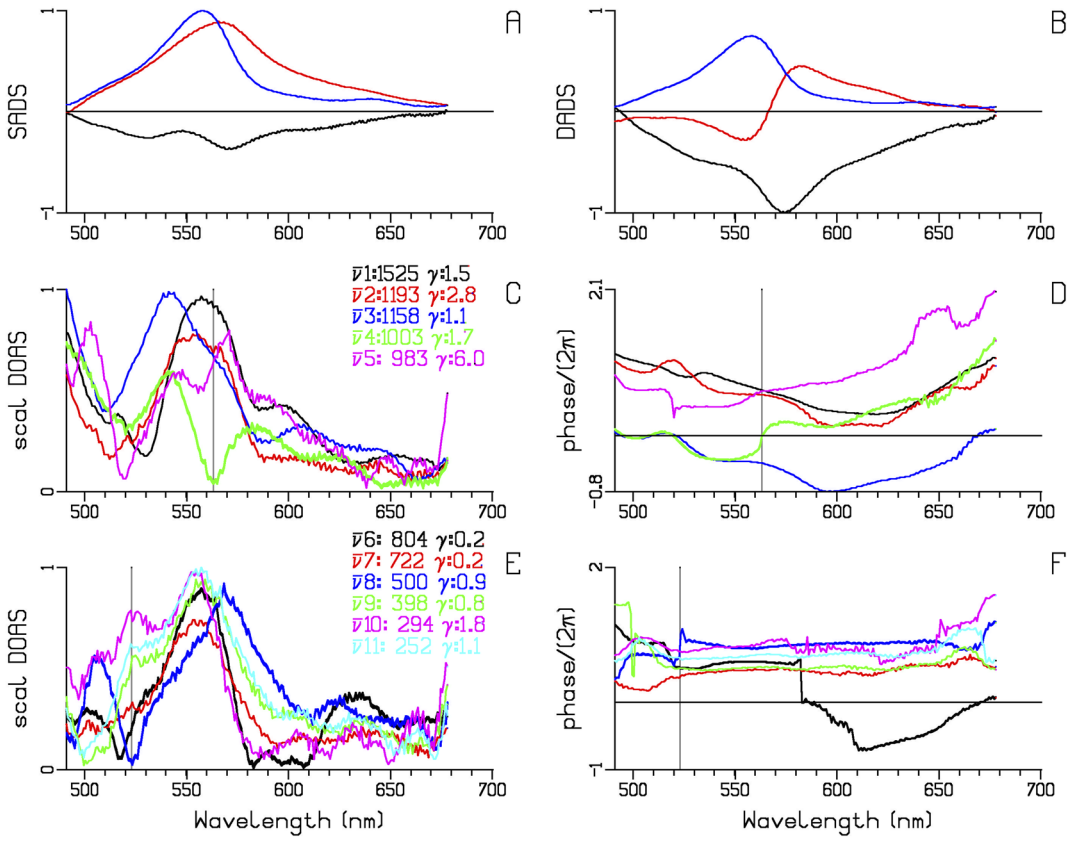

FIG. 6. DOAS analysis of β-carotene in cyclohexane excited with a 10 fs pulse centered at 560 nm and probed with an attenuated pulse from the Polli *et al.*[1] data. Estimated SADS (a) and DADS (b). Key (a) and (b): 168 fs (S2, black), 0.38 ps (hot S1, red), and 9.0 ps (S1, blue). Overview of selected estimated DOAS and phases. Frequencies $\bar{\nu}n$ (in cm^{-1}) (where n is the DOAS number) and damping rates γ (in ps^{-1}) written in the legend of panel (c) and (e) using the appropriate color. (c) and (e) Estimated DOAS, scaled for comparison. (d) and (f) Estimated phase profiles of the DOAS. The gray vertical lines at 563 nm in panels (c) and (d) and at 523 nm in panels (e) and (f) are discussed in the text.

Fig. 6(a), it was 77 mOD. Thus, we infer that the high energy tail of the pump pulse was overlapping with a smaller part of the red-most β-carotene absorption [Figs. S1(A) and S2] and that in Polli *et al.*[1] some more blue absorbing molecules have been excited. Selected estimated DOAS are plotted in Figs. 7(c) and 7(e) and Figs. S12(H), S12(K), and S12(N). Several nodes accompanied by phase jumps are visible: (a) with the 1526 cm^{-1} (No. 4, red, damping rate 1.8 ps^{-1}) at 630 nm [Figs. 7(c) and 7(d)], (b1) with the 803 cm^{-1} (No. 10, green, damping rate 0.2 ps^{-1}) at ≈665 nm, and (b2) with the 1265 cm^{-1} (No. 5, red, damping rate 1.5 ps^{-1}) at ≈606 nm [cf., the gray vertical lines in Figs. 7(e) and 7(f)]. Apart from the cyclohexane Raman ISRS near 803 cm^{-1}, the DOAS represent the vibronic dynamics of the excited β-carotene. Thus, although some of the estimated frequencies are common between the data of Polli *et al.*[1] and Liebel and Kukura[2], the DOAS patterns differ, reflecting the different excitation patterns of the molecules. A second experiment by Liebel of β-carotene in cyclohexane with slightly different pulse properties demonstrates the reproducibility of the results, cf., the discussion around Figs. S13–S15. Comparing the SADS in Figs. 6(a) and 7(a) and Fig. S14, the hot S1 state is of somewhat lower energy in the Liebel and Kukura data,[2] resulting in a slight blue shift of the hot S1 ESA, cf., the red, orange, and magenta SADS in Fig. 8(a). It is striking that the red, orange, and magenta DADS cross zero near 565 nm, coincident with the maxima of the hot S1 SADS, representing the vibrational cooling [Fig. 8(b)]. Despite the different excitation conditions, the overall agreement of the DADS and the SADS in the experiments performed in different laboratories confirms the validity of the global and target analysis approach.

The contribution of the damped oscillations to the fit and the quality of the fit are demonstrated in Fig. S18 (for the data from Fig. 7) and in Fig. 9 for the 601 nm β-carotene in cyclohexane data in three different experiments. Here, we concentrate on the 0.1–1.1 ps time range, where the hot S1 state (red) is converted to the S1 state (blue). The DOAS method allows us to resolve the solvent contributions (ISRS, green and CA, cyan) from the contributions of the β-carotene damped oscillations (magenta). The amplitude decrease of the magenta signal correlates with the decay of the hot S1 state (red). This strongly suggests that vibrational coherence is maintained when going through the S2–S1 conical intersection and that

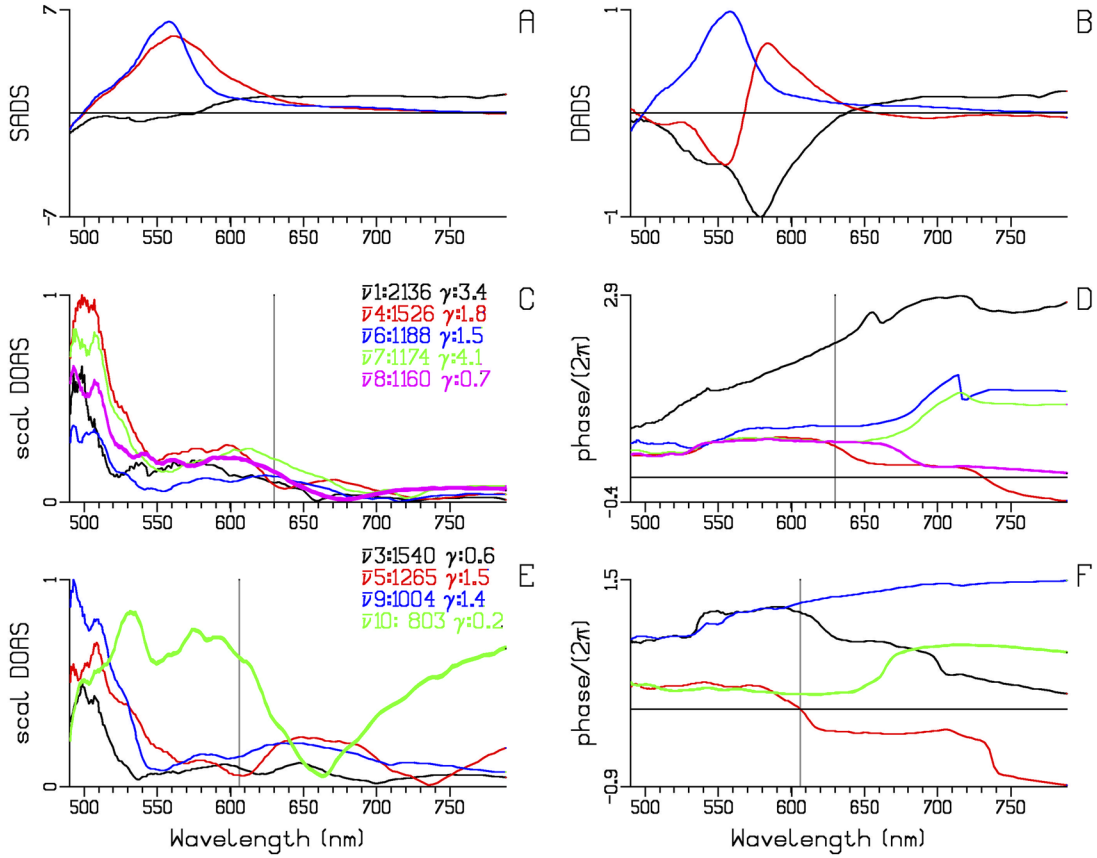

FIG. 7. DOAS analysis of β-carotene in cyclohexane excited with a 12 fs pulse centered at ≈570 nm and probed with a 5 fs pulse at 660 nm from the Liebel and Kukura[2] data. Estimated SADS (a) and DADS (b). Key (a) and (b): 199 (S2, black), 337 fs (hot S1, red), and 8.9 ps (S1, blue). Overview of selected estimated DOAS and phases. Frequencies $\bar{\nu}n$ (in cm^{-1}) (where n is the DOAS number) and damping rates γ (in 1 ps^{-1}) written in the legend of panel (c) and (e) using the appropriate color. (c) and (e) Estimated DOAS, scaled for comparison. (d) and (f) Estimated phase profiles of the DOAS. The gray vertical lines at 630 nm in panels (c) and (d) and at 606 nm in panels (e) and (f) are discussed in the text.

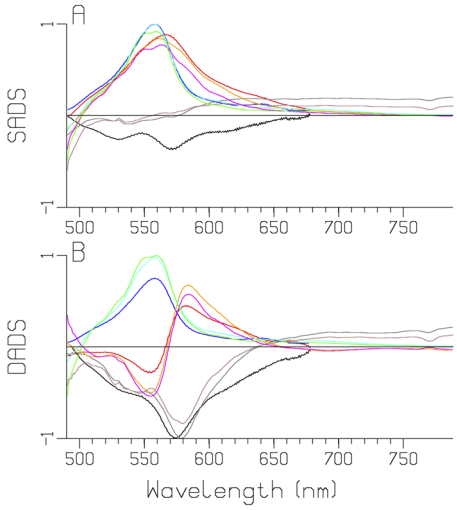

FIG. 8. Overlays of the SADS (a) and the DADS (b) (scaled to the extrema) estimated from the Polli *et al.*[1] data [key: 168 (S2, black), 0.38 ps (hot S1, red), and 9.0 ps (S1, blue)] and from the Liebel and Kukura[2] data [key: 199 (gray, brown), 337 (orange, magenta) fs, and 8.9 ps (cyan, green)]. The gray, orange, and cyan curves are from the first Liebel experiment, Figs. 7(a) and 7(b), whereas the brown, magenta, and green curves are from the second Liebel experiment, Figs. S14(B) and S14(C).

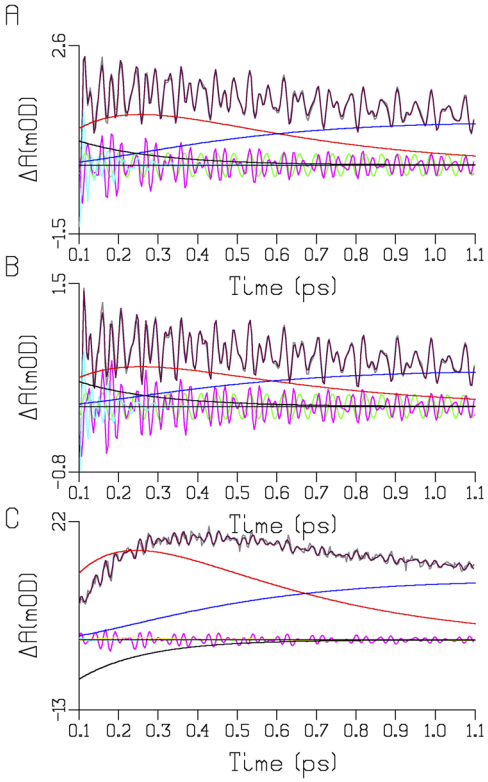

FIG. 9. Decomposition of the 601 nm β-carotene in cyclohexane data (in mOD, gray, and the fit, maroon). Key excited state contributions: S2, black; hot S1, red; and S1, blue. Key damped oscillations: green is the 803 cm^{-1} cyclohexane ISRS, cyan is the sum of the CA damped oscillations (decay rates: 20–25 ps^{-1}), and magenta is the sum of all the β-carotene damped oscillations (i.e., without any cyclohexane contribution). (a) and (b) First and second Liebel experiment and (c) Polli experiment.

we are directly observing the vibrational relaxation and nuclear reorganization[71] responsible for the hot S1 to S1 transition. Strikingly, we observe a wavepacket with a pitch-like periodicity in the magenta signal. The frequencies of the largest DOAS, 1526 and 1174 cm^{-1} [red and green in Figs. 7(c) and 7(d)] result in a pitch frequency of 1526 − 1174 = 352 cm^{-1} that corresponds to a periodicity of 95 fs, which is present in the magenta signals in all three panels of Fig. 9. Note that there is a missing fundamental, since no ≈352 cm^{-1} damped oscillation is observed.

DOAS interpretation

The CA could largely be described with the help of a Gaussian shape and its first and second derivatives and the IRFAS, cf., Figs. 2(c) and 2(d) [see also the panels (D) and (E) of Figs. S3, S4, S10, S12, S14, and S16]. In general, all three contribute, and in some cases, the second derivative contribution is clearly visible already in the data. In addition to those, five DOAS with faster damping rates are needed to fit the CA [Figs. 2(e) and 2(f)]. Now that the IRF and the CA are fully taken into account, many more damped oscillations can be resolved. The frequencies of the DOAS with damping rates smaller than 10 ps^{-1} most probably correspond to properties of the molecular system. It is striking that the temporal width parameter of the CA Δ', required to successfully model the data, is more than twice as large as the width parameter Δ of the IRF (Table II).

The DOAS are analogous to DADS and can directly be interpreted as the amplitude of a given coherent oscillation, with a defined phase and dephasing lifetime, as a function of the detection wavelength. The DOAS reveal clearly visible nodes, with corresponding phase change, which flag the minimum of the PES in which the oscillation occurs. This location is where, due to interference effects, oscillations cancel.[28] In the relatively simple all-trans β-carotene system, some of the damping rates corresponded to the rates of the S2 → hot S1 → S1 transitions.

DOAS can be attributed to both electronically excited states and to the ground state [cf., Fig. S7(B)]. Selected DOAS of all-trans β-carotene in cyclohexane are collated in Fig. 10. Some assignments of the modes can be based upon the frequencies estimated from transient Raman bands of β-carotene in cyclohexane (Table IV).[72] DOAS with frequencies near 1525, 1158, and 1003 cm^{-1} are shown in black, blue, and green in Figs. 10(a)–10(d). These DOAS are strikingly different between the two experiments, which can be attributed to the different vibronic excitation patterns and probably also to the different properties of the probe pulse. There is a higher amount of excess excitation energy in the experiment of Polli *et al.*[1] [Figs. S1(A) and S2], causing a much larger maximum SADS amplitude (77 vs 6.2 mOD, Table II). Relatively, the oscillations are larger with Liebel, cf., Fig. 9, probably also because the small overlap of the ISRS pulse with the β-carotene absorption selects only the redmost absorbing states, whereas the larger overlap with Polli will excite a heterogeneous mixture.

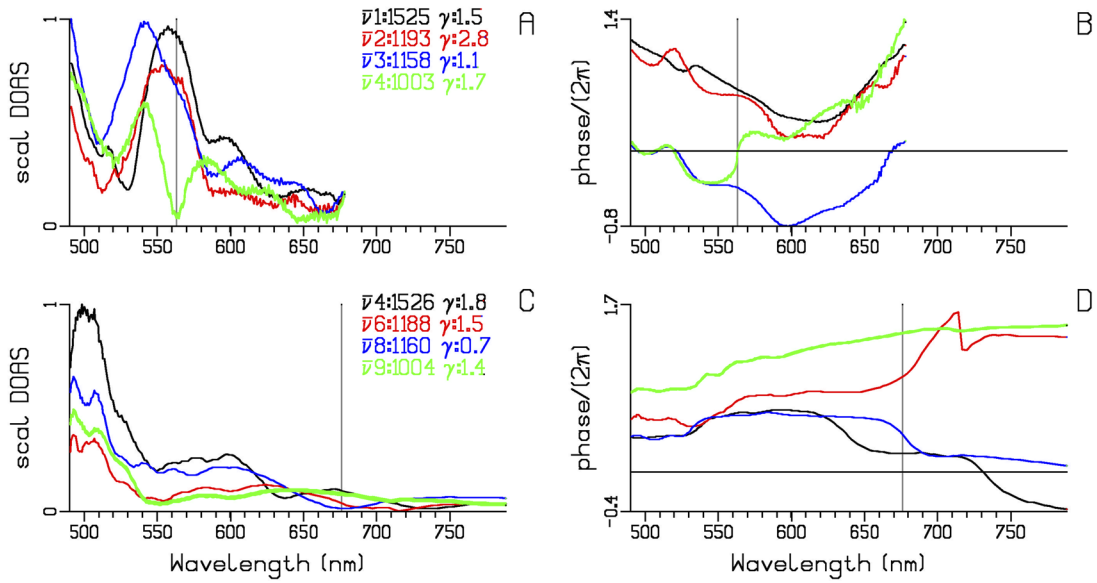

FIG. 10. Comparison of selected DOAS of all-trans β-carotene in cyclohexane from the experiments of Polli *et al.*[1] (a) and (b) and Liebel and Kukura[2] (c) and (d). Frequencies $\bar{\nu}n$ (in cm^{-1}) (where n is the DOAS number) and damping rates γ (in ps^{-1}) written in the legend of panel (a), (c), and (e) using the appropriate color. (a) and (c) Estimated DOAS, scaled for comparison. (b) and (d) Estimated phase profiles of the DOAS. The gray vertical lines at 565 nm in panels (a) and (b) and at 676 nm in panels (c) and (d) are discussed in the text.

The assignment cannot be based just upon the frequency but must take into account the full DOAS and phase characteristic and the damping rate. Most interesting are modes that are damped with rates close to the decay rates of the electronically excited states.[49,50,71]

In Ref. 1, the oscillations are ascribed to a vibrational wavepacket launched on the ground state PES. Here, we find a mode at 983 cm^{-1}, with a decay rate of 6.0 ps^{-1} [magenta curves in Figs. 6(c) and 6(d)]. Its DOAS has a broad maximum around 570 nm. The node at 520 nm is accompanied by an $\approx\pi$-phase jump. Whether this mode is involved in vibrational relaxation of hot S1 will be investigated further. Additionally, the intriguing observations of wavepackets damped during the vibrational relaxation of hot S1 (Fig. 9) will be investigated further.

After preparation of a β-carotene S1 state by a prepulse at 460 nm, a 137 cm^{-1} mode, No. 13 [blue in Figs. S19(M)–S19(O)] is damped with 2.9 ps^{-1}, and also the 1800 and 1525 cm^{-1} modes are damped with 3.0 and 2.8 ps^{-1} [blue and magenta in Figs. S19(G)–S19(I)]. All three modes can be interpreted as vibrational relaxation, since the damping rates are comparable to the decay rate of hot S1.

These observations demonstrate that the above-described modes are context dependent.

The observation that vibrational coherence is maintained (Fig. 9) when going through the S2–S1 conical intersection is reminiscent of the vibrationally coherent photochemistry in rhodopsin.[73,74]

Previously, Fourier transform maps of the dataset well after the IRF were used to identify oscillations and their phase character.[2,27,29,38,47,75] In addition to resolving significantly more oscillations, at the frequencies that characterize the system, the enhanced DOAS method very clearly reveals the unique nodal features, phase profiles, and dephasing times for each of them. This represents the most detailed and complete analysis of vibrational coherence in all-trans β-carotene, fit simultaneously with its population dynamics, in the time domain from complete TA datasets.

The placement of nodes in the data allows certain assignments of the DOAS in the excited states PESs in all-trans β-carotene. Overall, we can see that both ground state and excited state coherences are generated, as expected from impulsive excitation with a broadband pulse.[23,25] Our simulations for Nile blue suggest that the excited state contribution dominates (Fig. S7).

TABLE IV. Provisional assignment of modes from transient Raman bands of β-carotene in cyclohexane according to Ref. 72.

State\mode (cm^{-1})	C=C stretch, $\bar{\nu}1$	C–C stretch, $\bar{\nu}2$	$C–CH_3$ methyl rock, $\bar{\nu}3$
S0	1524	1156	1004
S1	1790	1250	1011
Hot S0	1512	1145	

Global analysis of FSRS measurements of all-trans β-carotene

FSRS[49,50,72,76] is complementary to broadband TA spectroscopy. For comparison with the above analyzed measurements, β-carotene in cyclohexane was excited with a 495 nm pulse, the

FWHM of the IRF was ≈127 fs. Thus, one can observe the Raman difference spectrum during the evolution from the S2 to S1 state. Using a sequential scheme S2 → hot S1 → S1′ → S1 → S0 with lifetimes of 167 fs (fixed), 0.35, 1.1 and 9.6 ps, we estimated the SADS of Fig. 11. During the relaxation of hot S1 to S1 another intermediate S1′ was resolved, which was not resolved in the TA spectral evolution. The third SADS (Fig. 11, blue) can be attributed to almost relaxed S1,[52] based upon the S1 peak around 1784 cm^{-1}. It evolves in 1.1 ps to the relaxed S1 peaking around 1792 cm^{-1}, which has a lifetime of 9.6 ps, consistent with the S1 lifetimes estimated above. Between 820 and 2100 cm^{-1}, we recognize the familiar bleach signals (corresponding to negative bands in the SADS) near 1519, 1150, and 1017 cm^{-1} that can be attributed to the bleach of the C=C stretch, C–C stretch, and C–CH_3 methyl rock of S0. Additional bleach signals are visible near 1440, 1262, and 1344 cm^{-1} and very small bands near 2048, 1581, and 1184 cm^{-1}. The excited S2 (black SADS) shows excess absorption near 1900 and 1300 cm^{-1}. The next state, which decays with a 0.35 ps time constant (red), shows a large excess absorption from 820 to 1000 cm^{-1} and from 1550 to 1680 cm^{-1} and small bands around 1370 and 2000 cm^{-1} [Fig. 11(b)]. It is ascribed to hot S1. These bands that decay with a rate of 2.9 ps^{-1} may be involved in the vibrational relaxation and nuclear reorganization[71] responsible for the hot S1 to S1 transition. The small bands around 1970 cm^{-1} may correspond to the DOAS Nos. 1 and 2, black and red in Figs. S19(G)–S19(I).

The FSRS signals straddling time zero are highly complex and can be described with contributions from the IRF and its derivatives (Fig. S21), and with damped oscillations, mainly decaying time-reversedly (Fig. S22). A 94 cm^{-1} DOAS has been resolved [Figs. S21(D)–S21(F)], with amplitude mainly below 1000 cm^{-1}, which was the region where the hot S1 showed large amplitudes as well [Figs. S20 and S21(A)]. This suggests that a wavepacket is present during the S2 → hot S1 → S1′ transitions.

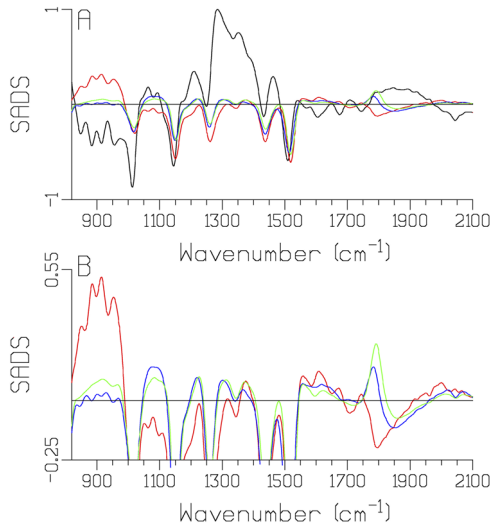

FIG. 11. SADS from FSRS of β-carotene in cyclohexane excited with a low intensity 495 nm pulse. Key: 167 fs (fixed, black), 0.35 (red), 1.1 (blue), and 9.6 ps (green). Panel (b) is a magnification of panel (a), omitting the first SADS.

CONCLUSION

In this work, we have presented an enhanced DOAS methodology that fits all the available experimental data, including the coherent artifact around time zero, and fully takes into account the IRF of the system. It is applicable to broadband TA of both relatively simple (this work) and complex[40–42] systems. Our analytical approach delivers a complete description of the time evolution of the electronically and vibrationally excited states. We provide examples of its application to several high time resolution TA experiments, which highlight its capability to fully describe the data and extract their rich spectroscopic information.

The fs–ps dynamics of β-carotene in cyclohexane in TA and FSRS experiments can be described by a sequential scheme S2 → hot S1 → S1′ → S1 → S0 with lifetimes of 167 fs (fixed), 0.35, 1.1, and 9.6 ps. The correspondence of DOAS decaying concomitantly with hot S1 and the SADS of hot S1 in TA and FSRS suggest that we are observing here features of the vibrational relaxation and nuclear reorganization[71] responsible for the hot S1 to S1 transition. The enhanced DOAS methodology thus allows one to follow and quantify the coherent dynamics of the vibronic wavepacket while undergoing strongly non-adiabatic dynamics such as passing through the conical intersection. We envisage that this methodology could become a standard tool to analyze the complex vibrational wavepacket dynamics on multidimensional PES produced in high time resolution TA experiments.

SUPPLEMENTARY MATERIAL

See the supplementary material for 22 figures demonstrating the properties of the pulses, the quality of the fit, details of the Nile blue DOAS simulation, the reproducibility, the DOAS analyses of two more TA experiments, and the complete DOAS analysis of the FSRS experiment.

ACKNOWLEDGMENTS

We are very grateful to Matz Liebel for generously sharing his data and for helpful discussions. We thank Mariangela Di Donato, Chanelle Jumper, Freek Ariese, Philipp Kukura, Pavel Malý, Joris Snellenburg, and René Williams for their interest and helpful discussions. We acknowledge funding from the European Union's Horizon 2020 research and innovation program under Grant Agreements Nos. 654148 and 871124 Laserlab-Europe.

There is no conflict of interest to declare.

DATA AVAILABILITY

The data that support the findings of this study are available from the corresponding author upon reasonable request.

REFERENCES

[1]D. Polli, M. R. Antognazza, D. Brida, G. Lanzani, G. Cerullo, and S. De Silvestri, "Broadband pump-probe spectroscopy with sub-10-fs resolution for probing ultrafast internal conversion and coherent phonons in carotenoids," Chem. Phys. **350**(1-3), 45–55 (2008).

[2]M. Liebel and P. Kukura, "Broad-band impulsive vibrational spectroscopy of excited electronic states in the time domain," J. Phys. Chem. Lett. **4**(8), 1358–1364 (2013).
[3]S. L. Dexheimer, Q. Wang, L. A. Peteanu, W. T. Pollard, R. A. Mathies, and C. V. Shank, "Femtosecond impulsive excitation of nonstationary vibrational states in bacteriorhodopsin," Chem. Phys. Lett. **188**(1-2), 61–66 (1992).
[4]A. H. Zewail, "Femtochemistry: Atomic-scale dynamics of the chemical bond," J. Phys. Chem. A **104**(24), 5660–5694 (2000).
[5]J. C. Dean, S. Rafiq, D. G. Oblinsky, E. Cassette, C. C. Jumper, and G. D. Scholes, "Broadband transient absorption and two-dimensional electronic spectroscopy of methylene blue," J. Phys. Chem. A **119**(34), 9098–9108 (2015).
[6]S. Rafiq and G. D. Scholes, "Slow intramolecular vibrational relaxation leads to long-lived excited-state wavepackets," J. Phys. Chem. A **120**(34), 6792–6799 (2016).
[7]J. Brazard, L. A. Bizimana, T. Gellen, W. P. Carbery, and D. B. Turner, "Experimental detection of branching at a conical intersection in a highly fluorescent molecule," J. Phys. Chem. Lett. **7**(1), 14–19 (2016).
[8]C. N. Lincoln, J. Hayden, A. G. Pour, V. Perlík, F. Šanda, and J. Hauer, "A quantitative study of coherent vibrational dynamics probed by heterodyned transient grating spectroscopy," Vib. Spectrosc. **85**, 167–174 (2016).
[9]M. H. Vos, J. C. Lambry, S. J. Robles, D. C. Youvan, J. Breton, and J. L. Martin, "Direct observation of vibrational coherence in bacterial reaction centers using femtosecond absorption spectroscopy," Proc. Natl. Acad. Sci. U. S. A. **88**(20), 8885–8889 (1991).
[10]D. M. Jonas, M. J. Lang, Y. Nagasawa, T. Joo, and G. R. Fleming, "Pump–probe polarization anisotropy study of femtosecond energy transfer within the photosynthetic reaction center of *Rhodobacter sphaeroides* R26," J. Phys. Chem. **100**(30), 12660–12673 (1996).
[11]S. Lin, A. K. W. Taguchi, and N. W. Woodbury, "Excitation wavelength dependence of energy transfer and charge separation in reaction centers from *Rhodobacter sphaeroides*: Evidence for adiabatic electron transfer," J. Phys. Chem. **100**(42), 17067–17078 (1996).
[12]S. Savikhin, Y. Zhu, S. Lin, R. E. Blankenship, and W. S. Struve, "Femtosecond spectroscopy of chlorosome antennas from the green photosynthetic bacterium *Chloroflexus aurantiacus*," J. Phys. Chem. **98**(40), 10322–10334 (1994).
[13]S. Savikhin, D. R. Buck, and W. S. Struve, "Oscillating anisotropies in a bacteriochlorophyll protein: Evidence for quantum beating between exciton levels," Chem. Phys. **223**(2-3), 303–312 (1997).
[14]M. Chachisvilis, T. Pullerits, M. R. Jones, C. N. Hunter, and V. Sundström, "Vibrational dynamics in the light-harvesting complexes of the photosynthetic bacterium *Rhodobacter sphaeroides*," Chem. Phys. Lett. **224**(3-4), 345–354 (1994).
[15]W. M. Diffey, B. J. Homoelle, M. D. Edington, and W. F. Beck, "Excited-state vibrational coherence and anisotropy decay in the bacteriochlorophyll a dimer protein B820," J. Phys. Chem. B **102**(15), 2776–2786 (1998).
[16]E. J. Heller, "The semiclassical way to molecular spectroscopy," Acc. Chem. Res. **14**(12), 368–375 (1981).
[17]R. B. Bernstein and A. H. Zewail, "Femtosecond real-time probing of reactions. III. Inversion to the potential from femtosecond transition-state spectroscopy experiments," J. Chem. Phys. **90**(2), 829–842 (1989).
[18]C. Cohen-Tannoudji, B. Diu, and F. Lalöe, *Quantum Mechanics* (Wiley-Interscience, Paris, 1977).
[19]M. H. Vos, F. Rappaport, J.-C. Lambry, J. Breton, and J.-L. Martin, "Visualization of coherent nuclear motion in a membrane protein by femtosecond spectroscopy," Nature **363**(6427), 320–325 (1993).
[20]I. A. Walmsley, F. W. Wise, and C. L. Tang, "On the difference between quantum beats in impulsive stimulated Raman scattering and resonance Raman scattering," Chem. Phys. Lett. **154**(4), 315–320 (1989).
[21]C. J. Bardeen, Q. Wang, and C. V. Shank, "Femtosecond chirped pulse excitation of vibrational wave packets in LD690 and bacteriorhodopsin," J. Phys. Chem. A **102**(17), 2759–2766 (1998).
[22]C. J. Bardeen, Q. Wang, and C. V. Shank, "Selective excitation of vibrational wave packet motion using chirped pulses," Phys. Rev. Lett. **75**(19), 3410–3413 (1995).
[23]D. M. Jonas, S. E. Bradforth, S. A. Passino, and G. R. Fleming, "Femtosecond wavepacket spectroscopy: Influence of temperature, wavelength, and pulse duration," J. Phys. Chem. **99**(9), 2594–2608 (1995).
[24]W. T. Pollard and R. A. Mathies, "Analysis of femtosecond dynamic absorption spectra of nonstationary states," Annu. Rev. Phys. Chem. **43**(1), 497–523 (1992).
[25]A. S. Johnson, J. Yuen-Zhou, A. Aspuru-Guzik, and J. J. Krich, "Practical witness for electronic coherences," J. Chem. Phys. **141**(24), 244109 (2014).
[26]G. Lanzani, M. Zavelani-Rossi, G. Cerullo, D. Comoretto, and G. Dellepiane, "Real-time observation of coherent nuclear motion in polydiacetylene isolated chains," Phys. Rev. B **69**(13), 134302 (2004).
[27]P. C. Arpin, D. B. Turner, S. D. McClure, C. C. Jumper, T. Mirkovic, J. R. Challa, J. Lee, C. Y. Teng, B. R. Green, K. E. Wilk, P. M. G. Curmi, K. Hoef-Emden, D. W. McCamant, and G. D. Scholes, "Spectroscopic studies of cryptophyte light harvesting proteins: Vibrations and coherent oscillations," J. Phys. Chem. B **119**(31), 10025–10034 (2015).
[28]J. A. Cina, P. A. Kovac, C. C. Jumper, J. C. Dean, and G. D. Scholes, "Ultrafast transient absorption revisited: Phase-flips, spectral fingers, and other dynamical features," J. Chem. Phys. **144**(17), 175102 (2016).
[29]S. D. McClure, D. B. Turner, P. C. Arpin, T. Mirkovic, and G. D. Scholes, "Coherent oscillations in the PC577 cryptophyte antenna occur in the excited electronic state," J. Phys. Chem. B **118**(5), 1296–1308 (2014).
[30]S. Rafiq, J. C. Dean, and G. D. Scholes, "Observing vibrational wavepackets during an ultrafast electron transfer reaction," J. Phys. Chem. A **119**(49), 11837–11846 (2015).
[31]Q. Wang, R. Schoenlein, L. Peteanu, R. Mathies, and C. Shank, "Vibrationally coherent photochemistry in the femtosecond primary event of vision," Science **266**(5184), 422 (1994).
[32]D. B. Turner and P. C. Arpin, "Basis set truncation further clarifies vibrational coherence spectra," Chem. Phys. **539**, 110948 (2020).
[33]S. A. Kovalenko, A. L. Dobryakov, J. Ruthmann, and N. P. Ernsting, "Femtosecond spectroscopy of condensed phases with chirped supercontinuum probing," Phys. Rev. A **59**(3), 2369–2384 (1999).
[34]N. P. Ernsting, S. A. Kovalenko, T. Senyushkina, J. Saam, and V. Farztdinov, "Wave-packet-assisted decomposition of femtosecond transient ultraviolet–visible absorption spectra: Application to excited-state intramolecular proton transfer in solution," J. Phys. Chem. A **105**(14), 3443–3453 (2001).
[35]A. L. Dobryakov, S. A. Kovalenko, and N. P. Ernsting, "Electronic and vibrational coherence effects in broadband transient absorption spectroscopy with chirped supercontinuum probing," J. Chem. Phys. **119**(2), 988–1002 (2003).
[36]P. Hamm and M. Zanni, *Concepts and Methods of 2D Infrared Spectroscopy* (Cambridge University Press, 2011).
[37]A. Bresci, M. Guizzardi, C. M. Valensise, F. Marangi, F. Scotognella, G. Cerullo, and D. Polli, "Removal of cross-phase modulation artifacts in ultrafast pump–probe dynamics by deep learning," APL Photonics **6**(7), 076104 (2021).
[38]M. Liebel, C. Schnedermann, T. Wende, and P. Kukura, "Principles and applications of broadband impulsive vibrational spectroscopy," J. Phys. Chem. A **119**(36), 9506–9517 (2015).
[39]S. Ruetzel, M. Diekmann, P. Nuernberger, C. Walter, B. Engels, and T. Brixner, "Photoisomerization among ring-open merocyanines. I. Reaction dynamics and wave-packet oscillations induced by tunable femtosecond pulses," J. Chem. Phys. **140**(22), 224310 (2014).
[40]I. H. M. van Stokkum, C. C. Jumper, J. J. Snellenburg, G. D. Scholes, R. van Grondelle, and P. Malý, "Estimation of damped oscillation associated spectra from ultrafast transient absorption spectra," J. Chem. Phys. **145**(17), 174201 (2016).
[41]C. C. Jumper, I. H. M. van Stokkum, T. Mirkovic, and G. D. Scholes, "Vibronic wavepackets and energy transfer in cryptophyte light-harvesting complexes," J. Phys. Chem. B **122**(24), 6328–6340 (2018).
[42]I. H. M. van Stokkum, C. C. Jumper, T. S. Lee, M. Myahkostupov, F. N. Castellano, and G. D. Scholes, "Vibronic and excitonic dynamics in perylenediimide dimers and tetramer," J. Chem. Phys. **153**(22), 224101 (2020).
[43]S. Schott, L. Ress, J. Hrušák, P. Nuernberger, and T. Brixner, "Identification of photofragmentation patterns in trihalide anions by global analysis of vibrational wavepacket dynamics in broadband transient absorption data," Phys. Chem. Chem. Phys. **18**(48), 33287–33302 (2016).

[44]A. Volpato, L. Bolzonello, E. Meneghin, and E. Collini, "Global analysis of coherence and population dynamics in 2D electronic spectroscopy," Opt. Express **24**(21), 24773–24785 (2016).
[45]W. T. Pollard, H. L. Fragnito, J. Y. Bigot, C. V. Shank, and R. A. Mathies, "Quantum-mechanical theory for 6 fs dynamic absorption spectroscopy and its application to nile blue," Chem. Phys. Lett. **168**(3-4), 239–245 (1990).
[46]H. L. Fragnito, J.-Y. Bigot, P. C. Becker, and C. V. Shank, "Evolution of the vibronic absorption spectrum in a molecule following impulsive excitation with a 6 fs optical pulse," Chem. Phys. Lett. **160**(2), 101–104 (1989).
[47]M. Liebel, C. Schnedermann, and P. Kukura, "Vibrationally coherent crossing and coupling of electronic states during internal conversion in β-carotene," Phys. Rev. Lett. **112**(19), 198302 (2014).
[48]P. Kukura, D. W. McCamant, and R. A. Mathies, "Femtosecond stimulated Raman spectroscopy," Annu. Rev. Phys. Chem. **58**, 461–488 (2007).
[49]D. W. McCamant, P. Kukura, and R. A. Mathies, "Femtosecond time-resolved stimulated Raman spectroscopy: Application to the ultrafast internal conversion in β-carotene," J. Phys. Chem. A **107**(40), 8208–8214 (2003).
[50]P. Kukura, D. W. McCamant, and R. A. Mathies, "Femtosecond time-resolved stimulated Raman spectroscopy of the S_2 ($1B_u^+$) excited state of β-carotene," J. Phys. Chem. A **108**(28), 5921–5925 (2004).
[51]M. Kloz, J. Weißenborn, T. Polívka, H. A. Frank, and J. T. M. Kennis, "Spectral watermarking in femtosecond stimulated Raman spectroscopy: Resolving the nature of the carotenoid S^* state," Phys. Chem. Chem. Phys. **18**(21), 14619–14628 (2016).
[52]J. M. Artes Vivancos, I. H. M. van Stokkum, F. Saccon, Y. Hontani, M. Kloz, A. Ruban, R. van Grondelle, and J. T. M. Kennis, "Unraveling the excited-state dynamics and light-harvesting functions of xanthophylls in light-harvesting complex II using femtosecond stimulated Raman spectroscopy," J. Am. Chem. Soc. **142**(41), 17346–17355 (2020).
[53]Y. Hontani, M. Kloz, T. Polívka, M. K. Shukla, R. Sobotka, and J. T. M. Kennis, "Molecular origin of photoprotection in cyanobacteria probed by watermarked femtosecond stimulated Raman spectroscopy," J. Phys. Chem. Lett. **9**(7), 1788–1792 (2018).
[54]I. H. M. van Stokkum, D. S. Larsen, and R. van Grondelle, "Global and target analysis of time-resolved spectra," Biochim. Biophys. Acta **1657**, 82–104 (2004).
[55]I. H. M. van Stokkum, D. S. Larsen, and R. van Grondelle, "Erratum to "Global and target analysis of time-resolved spectra" [Biochimica et Biophysica Acta 1658/2–3 (2004) 82–104]," Biochim. Biophys. Acta **1658**, 262 (2004).
[56]G. P. M. Poppe and C. M. J. Wijers, "More efficient computation of the complex error function," ACM Trans. Math. Software **16**(1), 38–46 (1990).
[57]S. G. Johnson, Faddeeva package, http://ab-initio.mit.edu/wiki/index.php/Faddeeva_Package.
[58]C. H. Brito Cruz, J. P. Gordon, P. C. Becker, R. L. Fork, and C. V. Shank, "Dynamics of spectral hole burning," IEEE J. Quantum Electron. **24**(2), 261–269 (1988).
[59]P. C. Andrikopoulos, Y. Liu, A. Picchiotti, N. Lenngren, M. Kloz, A. S. Chaudhari, M. Precek, M. Rebarz, J. Andreasson, J. Hajdu, B. Schneider, and G. Fuertes, "Femtosecond-to-nanosecond dynamics of flavin mononucleotide monitored by stimulated Raman spectroscopy and simulations," Phys. Chem. Chem. Phys. **22**(12), 6538–6552 (2020).
[60]Y. Hontani, K. Inoue, M. Kloz, Y. Kato, H. Kandori, and J. T. M. Kennis, "The photochemistry of sodium ion pump rhodopsin observed by watermarked femto- to submillisecond stimulated Raman spectroscopy," Phys. Chem. Chem. Phys. **18**(35), 24729–24736 (2016).
[61]Y. Hontani, M. Broser, M. Luck, J. Weissenborn, M. Kloz, P. Hegemann, and J. T. M. Kennis, "Dual photoisomerization on distinct potential energy surfaces in a UV-absorbing rhodopsin," J. Am. Chem. Soc. **142**(26), 11464–11473 (2020).
[62]Y. X. Yan, E. B. Gamble, and K. A. Nelson, "Impulsive stimulated scattering: General importance in femtosecond laser pulse interactions with matter, and spectroscopic applications," J. Chem. Phys. **83**(11), 5391–5399 (1985).
[63]U. Banin, A. Bartana, S. Ruhman, and R. Kosloff, "Impulsive excitation of coherent vibrational motion ground surface dynamics induced by intense short pulses," J. Chem. Phys. **101**(10), 8461–8481 (1994).
[64]S. Ruhman, A. G. Joly, and K. A. Nelson, "Time-resolved observations of coherent molecular vibrational motion and the general occurrence of impulsive stimulated scattering," J. Chem. Phys. **86**(11), 6563–6565 (1987).
[65]J. Jose and K. Burgess, "Benzophenoxazine-based fluorescent dyes for labeling biomolecules," Tetrahedron **62**(48), 11021–11037 (2006).
[66]M. K. Lawless and R. A. Mathies, "Excited-state structure and electronic dephasing time of Nile blue from absolute resonance Raman intensities," J. Chem. Phys. **96**(11), 8037–8045 (1992).
[67]A. T. N. Kumar, F. Rosca, A. Widom, and P. M. Champion, "Investigations of amplitude and phase excitation profiles in femtosecond coherence spectroscopy," J. Chem. Phys. **114**(2), 701–724 (2001).
[68]L. W. Pickett, M. Muntz, and E. M. McPherson, "Vacuum ultraviolet absorption spectra of cyclic compounds. I. Cyclohexane, cyclohexene, cyclopentane, cyclopentene and benzene," J. Am. Chem. Soc. **73**(10), 4862–4865 (1951).
[69]A. L. Dobryakov and N. P. Ernsting, "Lineshapes for resonant impulsive stimulated Raman scattering with chirped pump and supercontinuum probe pulses," J. Chem. Phys. **129**(18), 184504 (2008).
[70]A. L. Dobryakov, J. L. Pérez Lustres, S. A. Kovalenko, and N. P. Ernsting, "Femtosecond transient absorption with chirped pump and supercontinuum probe: Perturbative calculation of transient spectra with general lineshape functions, and simplifications," Chem. Phys. **347**(1), 127–138 (2008).
[71]E. J. Taffet, B. G. Lee, Z. S. D. Toa, N. Pace, G. Rumbles, J. Southall, R. J. Cogdell, and G. D. Scholes, "Carotenoid nuclear reorganization and interplay of bright and dark excited states," J. Phys. Chem. B **123**(41), 8628–8643 (2019).
[72]S. Shim and R. A. Mathies, "Development of a tunable femtosecond stimulated Raman apparatus and its application to β-carotene," J. Phys. Chem. B **112**(15), 4826–4832 (2008).
[73]D. Polli, P. Altoè, O. Weingart, K. M. Spillane, C. Manzoni, D. Brida, G. Tomasello, G. Orlandi, P. Kukura, R. A. Mathies, M. Garavelli, and G. Cerullo, "Conical intersection dynamics of the primary photoisomerization event in vision," Nature **467**, 440 (2010).
[74]R. Schoenlein, L. Peteanu, R. Mathies, and C. Shank, "The first step in vision: Femtosecond isomerization of rhodopsin," Science **254**(5030), 412 (1991).
[75]C. Schnedermann, M. Liebel, and P. Kukura, "Mode-specificity of vibrationally coherent internal conversion in rhodopsin during the primary visual event," J. Am. Chem. Soc. **137**(8), 2886–2891 (2015).
[76]D. W. McCamant, J. E. Kim, and R. A. Mathies, "Vibrational relaxation in β-carotene probed by picosecond Stokes and anti-Stokes resonance Raman spectroscopy," J. Phys. Chem. A **106**(25), 6030–6038 (2002).